J|A|C|S
ARTICLES
Published on Web 06/06/2006

X-ray Absorption Edge Spectroscopy and Computational Studies on $LCuO_2$ Species: Superoxide−Cu^{II} versus Peroxide−Cu^{III} Bonding

Ritimukta Sarangi,[†] Nermeen Aboelella,[§] Kiyoshi Fujisawa,[#] William B. Tolman,[§] Britt Hedman,*[,‡] Keith O. Hodgson,*[,†,‡] and Edward I. Solomon*[,†]

Contribution from the Department of Chemistry, Stanford University, Stanford, California 94305, Stanford Synchrotron Radiation Laboratory, Stanford Linear Accelerator Center, Stanford University, Stanford, California 94309, Department of Biochemistry, Molecular Biology and Biophysics, University of Minnesota, St. Paul, Minnesota 55108, and Department of Chemistry, University of Tsukuba, Tsukuba 305-8571, Japan

Received March 5, 2006; E-mail: hedman@slac.stanford.edu; hodgson@slac.stanford.edu; edward.solomon@stanford.edu

Abstract: The geometric and electronic structures of two mononuclear CuO_2 complexes, [$Cu(O_2)$\{HB(3-Ad-5-^{i}Prpz)$_3$\}] (**1**) and [$Cu(O_2)$(β-diketiminate)] (**2**), have been evaluated using Cu K- and L-edge X-ray absorption spectroscopy (XAS) studies in combination with valence bond configuration interaction (VBCI) simulations and spin-unrestricted broken symmetry density functional theory (DFT) calculations. Cu K- and L-edge XAS data indicate the Cu(II) and Cu(III) nature of **1** and **2**, respectively. The total integrated intensity under the L-edges shows that the ψ^*_{LUMO}'s in **1** and **2** contain 20% and 28% Cu character, respectively, indicative of very covalent ground states in both complexes, although more so in **1**. Two-state VBCI simulations also indicate that the ground state in **2** has more Cu ($|3d^8\rangle$) character. DFT calculations show that the ψ^*_{LUMO} in both complexes is dominated by O_2^{n-} character, although the O_2^{n-} character is higher in **1**. It is shown that the ligand L plays an important role in modulating Cu−O_2 bonding in these $LCuO_2$ systems and tunes the ground states of **1** and **2** to have dominant Cu(II)−superoxide-like and Cu(III)−peroxide-like character, respectively. The contributions of ligand field (LF) and the charge on the absorbing atom in the molecule (Q^M_{mol}) to L- and K-edge energy shifts are evaluated using DFT and time-dependent DFT calculations. It is found that LF makes a dominant contribution to the edge energy shift, while the effect of Q^M_{mol} is minor. The charge on the Cu in the Cu(III) complex is found to be similar to that in Cu(II) complexes, which indicates a much stronger interaction with the ligand, leading to extensive charge transfer.

1. Introduction

Copper-containing enzymes play important roles in O_2 activation and reduction in biological systems. These include the trinuclear Cu site in laccase,[1] the binuclear Cu proteins, and the heteronuclear heme-Cu_B site present in cytochrome *c* oxidase.[2] The group containing the binuclear Cu sites is further divided into exchange-coupled and noncoupled classes on the basis of the magnetic interactions between the two copper sites.[3] The coupled binuclear proteins, which include hemocyanin, tyrosinase, and catechol oxidase, exhibit strong magnetic coupling ($-2J \leq 1200\ cm^{-1}$) and have been extensively studied using spectroscopic techniques.[4−7] Insight into the geometric and electronic structures of these sites has also been gained from studies on complexes that model the protein function of O_2 binding and activation to functionalize organic substrates.

Relative to the exchange-coupled proteins, less is known about the geometric and electronic structures of the noncoupled binuclear copper proteins. These include dopamine β-monooxygenase (DβM) and peptidylglycine α-hydroxylating monooxygenase (PHM), which utilize molecular O_2 to catalyze C−H bond hydroxylation in a stereospecific fashion (dopamine to norepinephrine in DβM and glycine backbone C−H hydroxylation in PHM).[8,9] Crystal structures of PHM have been solved and show that the Cu···Cu separation is ∼11 Å. This large separation precludes electronic coupling of the two copper centers.[8,10] The two Cu atoms are labeled Cu_M (ligated by

[†] Department of Chemistry, Stanford University.
[‡] Stanford Synchrotron Radiation Laboratory.
[§] University of Minnesota.
[#] University of Tsukuba.

(1) Solomon, E. I.; Sundaram, U. M.; Machonkin, T. E. *Chem. Rev.* **1996**, *96*, 2563−2605.
(2) Ferguson-Miller, S.; Babcock, G. T. *Chem. Rev.* **1996**, *96*, 2889−2907.
(3) Klinman, J. P. *Chem. Rev.* **1996**, *96*, 2541−2561.
(4) Solomon, E. I.; Chen, P.; Metz, M.; Lee, S. K.; Palmer, A. E. *Angew. Chem., Int. Ed.* **2001**, *40*, 4570−4590.
(5) Chen, P.; Solomon, E. I. *J. Inorg. Biochem.* **2002**, *88*, 368−374.
(6) Mirica, L. M.; Ottenwaelder, X.; Stack, T. D. P. *Chem. Rev.* **2004**, *104*, 1013−1045.
(7) Que, L., Jr.; Tolman, W. B. *Angew. Chem., Int. Ed.* **2002**, *41*, 1114−1137.
(8) Prigge, S. T.; Mains, R. E.; Eipper, B. A.; Amzel, L. M. *Cell Mol. Life Sci.* **2000**, *57*, 1236−1259.
(9) Kulathila, R.; Merkler, K. A.; Merkler, D. J. *Nat. Prod. Rep.* **1999**, *16*, 145−154.
(10) Prigge, S. T.; Kolhekar, A. S.; Eipper, A.; Amzel, L. M. *Biophys. J.* **1997**, *72*, WAMB9.

10.1021/ja0615223 CCC: $33.50

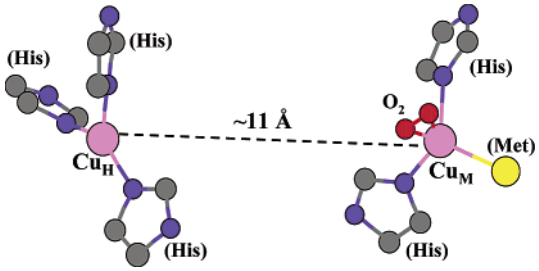

Figure 1. Pre-catalytic active site of peptidylglycine *R*-hydroxylating monooxygenase (PHM), showing the binuclear Cu site separated by ~11 Å. The O_2 is bound asymmetrically to the Cu_M site.

S(Met) and two N(His)) and Cu_H (ligated by three N(His)). O_2 binding and reduction occur at Cu_M, while Cu_H transfers one electron to the Cu_M site to complete the two-electron reduction of O_2 required for the reaction. It has been shown that the copper atoms cycle between a $Cu_M^ICu_H^I$ form and a $Cu_M^{II}Cu_H^{II}$ form in the reaction mechanism. Although various experimental and theoretical studies have been performed on both PHM and DβM,[3,11−14] the mechanism of the long-range electron transfer from Cu_H to Cu_M and O_2 reduction is unclear. Various mechanisms have been proposed, including superoxide channeling,[15] substrate-binding-mediated electron transfer to generate a hydroxide intermediate for two-electron reduction of O_2,[16,17] and direct H-atom abstraction by a one-electron-reduced superoxide intermediate.[5,11,12]

Recently, the $Cu_M(O_2)$ (plus slow substrate) intermediate has been trapped and the crystal structure determined (Figure 1).[18] This has triggered interest in characterizing synthetic models using spectroscopic methods which help understand various aspects of the protein chemistry. Two model complexes have been structurally characterized, [Cu(O_2){HB(3-*t*Bu-5-^{i}Prpz)$_3$}] (where HB(3-*t*Bu-5-^{i}Prpz)$_3$ = hydrotris(3-*tert*-butyl-5-isopropyl-1-pyrazolyl)borate, **1**)[19] and [Cu(O_2)(β-diketiminate)] (where β-diketiminate = *N*,*N*′-bis(2,6-diisopropylphenyl)-2,2,6,6-tetramethyl-3,5-pentanediiminato, **2**)[20] (Figure 2). A variation of **2** with an anilido-imine ligand system has also been structurally characterized,[21] and the results corroborate the structural data for **2**. Spectroscopic and theoretical characterization of **1** elucidated some aspects of O_2 binding and activation by a single copper center.[22] **2** is structurally similar to **1** in that it also has a side-on (η^2) binding mode of O_2 to Cu. However, these molecules differ dramatically in their spectroscopic properties. **1** has been described using magnetic susceptibility, electronic absorption, vibrational spectroscopy, and density functional

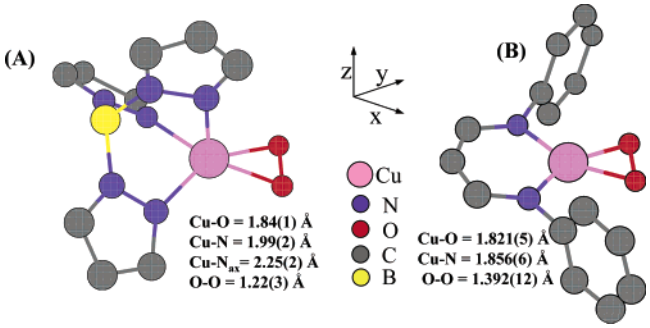

Figure 2. Crystal structures of **1** (A) and **2** (B). The ^{i}Pr and ^{t}Bu groups on the pyrazole ring and β-diketiminate ligand systems have been removed for clarity. Refer to text for bond length parameters.

theory (DFT) calculations as a highly covalent singlet species with no spin polarization in the ground state. The O−O stretching frequency in **1** is 1043 cm^{-1}, which is similar to those of well-characterized superoxide species.[23,24] In contrast, **2** has an O−O stretching frequency at 948 cm^{-1}, indicating considerable peroxide (O_2^{2-}) character.[20,25] Cu K-edge X-ray absorption studies on **2** indicate that the copper is in the 3+ oxidation state.[26] DFT calculations support the resonance Raman studies and indicate that **1** and **2** have predominant peroxide- and superoxide-like character, respectively.[20,22,26,27] These differences in two structurally analogous molecules hold potentially important information on O_2 binding and activation by the mononuclear Cu_M site.

Cu L-edge X-ray absorption spectroscopy (XAS) is a direct probe of the charge on the absorbing metal (M) in a molecule (Q^M_{mol}) and the ligand field (LF) of the Cu center.[28,29] L-edges are associated with the 2p→3d transition and have significant intensity due to their electric-dipole-allowed nature ($\Delta l = +1$). For Cu this transition occurs at ~930 eV. Additionally, relative to Cu K-edges (~9000 eV), the resolution at ~930 eV is much higher (0.1 eV compared to ~1 eV), which results in sharp, well-separated peaks.[30] In the case of most d^n ($n < 9$) species, the L-edge spectrum is rich in multiplet structure.[31] To interpret the L-edge spectra, the atomic terms need to be evaluated for both the initial and final configurations. In a molecular system, the atomic Hamiltonian is combined with ligand field terms using perturbation theory (see Experimental Section for details). Finally, the L-edges of highly covalent systems need an additional charge-transfer term in the Hamiltonian to include the effects of ground-state covalency and electronic relaxation due to the 2p→3d excitation.

In this study, our Cu K-edge study of **2**[26] has been extended to include the Cu K-edge of **1** and the Cu L-edges of **1** and **2**. These data are analyzed with a valence bond configuration interaction (VBCI) model, DFT, and time-dependent (TD)-

(11) Chen, P.; Solomon, E. I. *J. Am. Chem. Soc.* **2004**, *126*, 4991−5000.
(12) Chen, P.; Bell, J.; Eipper, B. A.; Solomon, E. I. *Biochemistry* **2004**, *43*, 5735−5747.
(13) Evans, J. P.; Ahn, K.; Klinman, J. P. *J. Biol. Chem.* **2003**, *278*, 49691−49698.
(14) Francisco, W. A.; Blackburn, N. J.; Klinman, J. P. *Biochemistry* **2003**, *42*, 1813−1819.
(15) Jaron, S.; Blackburn, N. J. *Biochemistry* **1999**, *38*, 15086−15096.
(16) Bell, J.; El Meskini, R.; D'Amato, D.; Mains, R. E.; Eipper, B. A. *Biochemistry* **2003**, *42*, 7133−7142.
(17) Prigge, S. T.; Kolhekar, A. S.; Eipper, B. A.; Mains, R. E.; Amzel, L. M. *Nat. Struct. Biol.* **1999**, *6*, 976−983.
(18) Prigge, S. T.; Eipper, B. A.; Mains, R. E.; Amzel, L. M. *Science* **2004**, *304*, 864−867.
(19) Fujisawa, K.; Tanaka, M.; Moro-oko, Y.; Kitajima, N. *J. Am. Chem. Soc.* **1994**, *116*, 12079−12080.
(20) Aboelella, N. W.; Lewis, E. A.; Reynolds, A. M.; Brennessel, W. W.; Cramer, C. J.; Tolman, W. B. *J. Am. Chem. Soc.* **2002**, *124*, 10660−10661.
(21) Reynolds, A. M.; Gherman, B. F.; Cramer, C. J.; Tolman, W. B. *Inorg. Chem.* **2005**, *44*, 6989−6997.
(22) Chen, P.; Root, D. E.; Campochiaro, C.; Fujisawa, K.; Solomon, E. I. *J. Am. Chem. Soc.* **2003**, *125*, 466−474.
(23) Andrews, L.; Smardzewski, R. R. *J. Chem. Phys.* **1973**, *58*, 2258−2261.
(24) Smardzewski, R. R.; Andrews, L. *J. Chem. Phys.* **1972**, *57*, 1327−1333.
(25) Spencer, D. J. E.; Aboelella, N. W.; Reynolds, A. M.; Holland, P. L.; Tolman, W. B. *J. Am. Chem. Soc.* **2002**, *124*, 2108−2109.
(26) Tolman, W. B.; et al. *J. Am. Chem. Soc.* **2004**, *126*, 16896−16911.
(27) Cramer, C. J.; Tolman, W. B.; Theopold, K. H.; Rheingold, A. L. *Proc. Natl. Acad. Sci. U.S.A* **2003**, *100*, 3635−3640.
(28) DeBeer George, S.; Metz, M.; Szilagyi, R. K.; Wang, H. X.; Cramer, S. P.; Lu, Y.; Tolman, W. B.; Hedman, B.; Hodgson, K. O.; Solomon, E. I. *J. Am. Chem. Soc.* **2001**, *123*, 5757−5767.
(29) George, S. J.; Lowery, M. D.; Solomon, E. I.; Cramer, S. P. *J. Am. Chem. Soc.* **1993**, *115*, 2968−2969.
(30) de Groot, F. *Chem. Rev.* **2001**, *101*, 1779−1808.
(31) de Groot, F. *Coord. Chem. Rev.* **2005**, *249*, 31−63.

DFT[32,33] calculations to understand the electronic structures of these molecules. The role of the ligand L in tuning these $LCuO_2$ systems toward more superoxide- or peroxide-like character has been explored. Comparison of **1** and **2** provides insight into the electronic structure of a Cu(III) site in a highly covalent ligand environment. This study utilizes metal K- and L-edge spectroscopies to understand the changes in Q^M_{mol} and LF of the metal center upon a one-electron oxidation of Cu(II) species.

2. Experimental Section

2.1. Samples. $[Cu(O_2)\{HB(3\text{-}Ad\text{-}5\text{-}^iPrpz)_3\}]$ (where HB(3-Ad-5-^{i}Prpz)$_3$ = hydrotris(3-adamantyl-5-isopropyl-1-pyrazolyl)borate, ^{1}L[34]) and $[Cu(O_2)(\beta\text{-diketiminate})]$ (where β-diketiminate = *N*,*N*′-bis(2,6-diisopropylphenyl)-3,5-methyldiiminato, ^{2}L) have been studied as analogues of **1** and **2** since they have greater thermal stability. The $[^1LCu(O_2)]$ (**1**)[19] and $[^2LCu(O_2)]$ (**2**)[26] complexes were synthesized as previously described. Both complexes are temperature sensitive (rate of decomposition highly enhanced above ~ −40 °C) and were handled in a glovebag under inert N_2 atmosphere and at dry ice temperatures during sample preparation. For Cu K-edge XAS, the solid samples were finely ground with BN into a homogeneous mixture and pressed into a 1 mm aluminum spacer between X-ray-transparent Kapton tape. The samples were immediately frozen and stored under liquid N_2. During data collection, the samples were maintained at a constant temperature of 10 K using an Oxford Instruments CF 1208 liquid helium cryostat. The Cu L-edge samples were similarly treated and spread thinly over double-sided adhesive conducting graphite tape on an Al sample paddle. The paddles were transferred onto a magnetic manipulator in an antechamber pre-chilled with liquid N_2 and then transferred into the main chamber and affixed to an Al block, which was cooled through conduction by a continuous flow of liquid He into a Cu block in an internal cavity. The temperature was monitored using a Lakeshore temperature controller and maintained at 20 K during the course of data measurement. The samples were positioned at 45° to the incident beam. The room-temperature stable $[Cu(TMPA)(OH_2)](ClO_4)_2$[35] complex (**3**), included as a reference, was handled on the benchtop. The Cu K- and L-edge data for all samples were collected at similar temperatures.

2.2. X-ray Absorption Spectroscopy. 2.2.1. Cu K-Edge. The Cu K-edge X-ray absorption spectra of **1**, **2**, and **3** were measured at the Stanford Synchrotron Radiation Laboratory (SSRL) on the focused 16-pole 2.0 T wiggler beam line 9-3 and the unfocused 8-pole 1.8 T wiggler beam line 7-3 under standard ring conditions of 3 GeV and 60−100 mA. A Si(220) double-crystal monochromator was used for energy selection. A Rh-coated harmonic rejection mirror and a cylindrical Rh-coated bent focusing mirror were used for beam line 9-3, whereas the monochromator was detuned 50% at 9987 eV on beam line 7-3 to reject components of higher harmonics. The transmission mode was used to measure data to $k = 16$ Å^{-1}. Internal energy calibration was accomplished by simultaneous measurement of the absorption of a Cu foil placed between two ionization chambers situated after the sample. The first inflection point of the foil spectrum was fixed at 8980.3 eV. Data presented here are 2−4 scan averaged spectra, which were processed by fitting a second-order polynomial to the pre-edge region and subtracting this from the entire spectrum as background. A three-region spline of orders 2, 3, and 3 was used to model the smoothly decaying post-edge region. The data were normalized by subtracting the cubic spline and assigning the edge jump to 1.0 at 9000 eV using the SPLINE routine in the XFIT[36] suite of programs.

2.2.2. Cu L-Edge. Cu L-edge X-ray absorption spectra were recorded at SSRL on the 31-pole wiggler beam line 10-1 under ring operating conditions of 50−100 mA and 3 GeV with a spherical grating monochromator with 1000 lines/mm and set at 30 μm entrance and exit slits. Sample measurements were performed using the total electron yield mode, where the sample signal (I_1) was collected with a Galileo 4716 channeltron electron multiplier aligned to 45° relative to the copper paddle. The signal was flux-normalized (I_1/I_0) using the photocurrent of a gold grid reference monitor (I_0). Data for all samples were recorded in a sample chamber maintained below 10^{-6} Torr, isolated from the ultra-high vacuum beam line by a 1000 Å Al window. External energy calibration was accomplished by L-edge measurements on CuF_2 before and after the sample. The L_3 and L_2 peak maxima were assigned to 930.5 and 950.5 eV, respectively. The variance in this calibration energy measured prior to and after each sample scan was used to linearly shift the experimental spectra between calibration scans. Spectra presented here are 3−5 scan averages, which were processed by fitting a second-order polynomial to the pre-edge region and subtracting it from the entire spectrum as background, resulting in a flat post-edge. The data were normalized to an edge jump of 1.0 at 1000 eV. The data for **3** were fit using EDG_FIT.[37] The L_3 and L_2 pre-edges were modeled using 50:50 Lorentzian:Gaussian pseudo-Voigt band shapes, and the rising edges were modeled using arctangents. The total pre-edge intensity was calculated as $L_3 + L_2$. Fits to the data for **1** and **2** were more complicated due to the presence of shake-up transitions. Two arctangents were subtracted from the data, which were separated by $^3/_2\lambda_{L.S}$ (20.25 eV) and fixed with an L_3:L_2 intensity ratio of 2:1. The total integrated area was obtained between 930 and 950 eV. The total integrated area of the L-edge of **3** was also obtained for comparison to **1** and **2**.

2.3. Electronic Structure Calculations. Gradient-corrected (GGA) spin-unrestricted broken symmetry density functional theory calculations were carried out using the Gaussian03[38] package on a 2-cpu linux computer. As reported in ref 22, Chen et al. have found that a more reasonable description of **1** was obtained using the BP86 pure functional, which gives the correct energy ordering of the singlet and low-lying triplet excited states. Thus, the Becke88[39,40] exchange and Perdew86[41] correlation nonlocal functionals with Vosko−Wilk−Nusair local functionals,[42] as implemented in the software package BP86, were employed in this study to compare the electronic structure differences between **1** and **2**. The triple-ζ 6-311+G* and the double-ζ 6-31G*[43−45] basis sets were used on the Cu, O, and N atoms and the C and H atoms, respectively. Population analyses were performed by means of Weinhold's natural population analysis (NPA),[46−48] including the Cu 4p orbitals in the valence set. Wave functions were visualized and orbital contour plots were generated in Molden.[49] Compositions of molecular orbitals and overlap populations between molecular fragments were calculated using the AOMix program.[50,51] For **1**, the alkyl side chains on the

(32) Casida, M. E. *Recent Advances In Density Functional Methods*; World Scientific: Singapore, 1995.
(33) Stratmann, R. E.; Scuseria, G. E.; Frisch, M. J. *J. Chem. Phys.* **1998**, *109*, 8218.
(34) Fujisawa, K.; Ono, T.; Aoki, H.; Ishikawa, Y.; Miyashita, Y.; Okamoto, K.; Nakazawa, H.; Higashimura, H. *Inorg. Chem. Commun.* **2004**, *7*, 330−332.
(35) Nagao, H.; Komeda, N.; Mukaida, M.; Suzuki, M.; Tanaka, K. *Inorg. Chem.* **1996**, *35*, 6809−6815.
(36) Ellis, P. J.; Freeman, H. C. *J. Synchrotron. Radiat.* **1995**, *2*, 190−195.
(37) George, G. N. EXAFSPAK & EDG_FIT, 2000.
(38) Pople, J. A.; et al. *Gaussian 03*, revision C.02; Gaussian Inc.: Wallingford, CT, 2004.
(39) Becke, A. D. *Phys. Rev. A* **1988**, *38*, 3098−3100.
(40) Becke, A. D. *J. Chem. Phys.* **1993**, *98*, 5648−5652.
(41) Perdew, J. P. *Phys. Rev. B* **1986**, *33*, 8822−8824.
(42) Vosko, S. H.; Wilk, L.; Nusair, M. *Can. J. Phys.* **1980**, *58*, 1200−1211.
(43) Hariharan, P. C.; Pople, J. A. *Theor. Chim. Acta* **1973**, *28*, 213−222.
(44) Francl, M. M.; Pietro, W. J.; Hehre, W. J.; Binkley, J. S.; Gordon, M. S.; DeFrees, D. J.; Pople, J. A. *J. Chem. Phys.* **1982**, *77*, 3654−3665.
(45) Rassolov, V. A.; Pople, J. A.; Ratner, M. A.; Windus, T. L. *J. Chem. Phys.* **1998**, *109*, 1223−1229.
(46) Foster, J. P.; Weinhold, F. *J. Am. Chem. Soc.* **1980**, *102*, 7211−7218.
(47) Carpenter, J. E.; Weinhold, F. *THEOCHEM* **1988**, *46*, 41−62.
(48) Reed, A. E.; Curtiss, L. A.; Weinhold, F. *Chem. Rev.* **1988**, *88*, 899−926.
(49) Schaftenaar, G.; Noordik, J. H. *J. Comput.-Aided Mol. Des.* **2000**, *14*, 123−134.
(50) Gorelsky, S. I.; Lever, A. B. P. *J. Organomet. Chem.* **2001**, *635*, 187−196.
(51) Gorelsky, S. I. *AOMix*, Revision 6.05, 2004 (http://www.sg-chem.net/).

pyrazole rings were replaced by hydrogen atoms. For **2**, the isopropyl side chains on the benzene rings on the ligand and the methyl groups on the carbon backbone were replaced by hydrogen atoms.

The geometry optimization of the reference complexes $[Cu^{II}L]^{2-}$ and $[Cu^{III}L]^{-}$ and the single-point calculation on $[Cu^{III}L^*]^{-}$ (for L, see section 4.2.5) employed the BP86 functional with 6-311G* basis sets on Cu and N and 6-31G* basis sets on the rest of the atoms.

2.4. XAS Multiplet Calculations. Atomic multiplet calculations were carried out using the T.T Multiplet software package, developed by R. D. Cowan et al.[52] and modified by B. T. Thole. The output of an atomic multiplet calculation is subjected to a LF multiplet calculation, which applies an electrostatic field around the metal center and employs Butler's branching rules[53] to split the atomic multiplets. Covalency was then included through charge-transfer mixing, using a two-configuration VBCI model (program developed by Okada).[54] Atomic Slater integrals were used in all simulations.[55] With the inclusion of electronic relaxation ($Q - U = -2$ eV) (see section 4.1), the charge-transfer parameters model the shake-up intensity observed at higher energies relative to the main L_3 and L_2 pre-edge peaks. The plots were generated using the program integrated with the multiplet program. The spectral simulations were generated using 0.4 and 0.6 eV Lorentzian broadening contributions (to account for core−hole lifetime effects) to the L_3- and L_2-edges, respectively. The whole spectrum was then convoluted with a 0.4 eV Gaussian (to account for experimental broadening).

2.5. TD-DFT Calculations. The time-dependent density functional theory (TD-DFT) framework implemented in ORCA[56,57] was used to compute Cu K-edge (1s→3d), and Cu L-edge (2p→3d) transition energies. The Becke88 exchange and Perdew86 correlation nonlocal functionals were employed. The all-electron Gaussian basis sets used were those reported by the Ahlrichs group.[58,59] Accurate triple-ζ valence basis sets (TZV(P)), with one set of polarization functions on all the atoms, were used to perform spin-unrestricted single-point calculations. The basis set dependence was tested by repeating the calculations using 6-311G* [60−62] with polarization. The self-consistent field (SCF) calculations were set to a tight convergence criterion (10^{-7} E_h in energy, 10^{-6} E_h in the density change, and 10^{-6} in the maximum element of the DIIS error vector). The RI modification was not employed. The input structures for the TD-DFT calculation were obtained from the spin-unrestricted DFT calculations performed at the BP86 level in Gaussian using a 6-311G* basis set on the Cu and O atoms and a 6-31G* basis set on N, C, and H atoms.

3. Results

3.1. Cu K-Edge. The normalized Cu K-edge X-ray absorption spectrum of **1**, compared to that of **2**, is presented in Figure 3. The pre-edge and shake-down energies are given in Table 1. In a previous study, the Cu K-edge spectrum of **2** was used to determine the predominant Cu(III) character of the complex.[26] The Cu(II) K-edge consists of a weak pre-edge transition at ∼8979 eV before the onset of the rising edge. The pre-edge

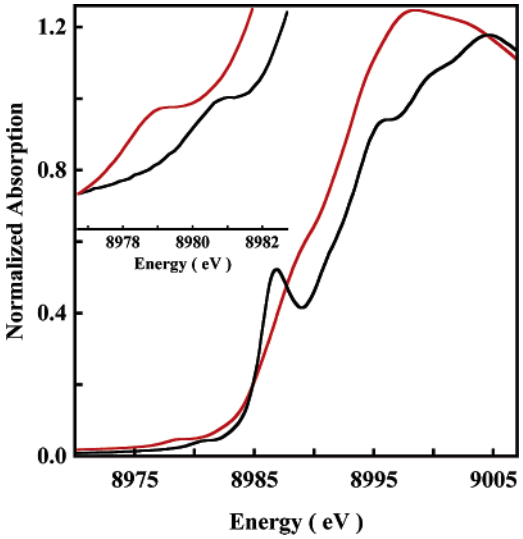

Figure 3. Normalized Cu K-edge XAS spectra of $[^1LCu(O_2)]$ (**1**, red line) and $[^2LCu(O_2)]$ (**2**, black line). Inset: Expanded pre-edge region (1s→3d transition), indicating a ∼2 eV shift.

corresponds to a dipole-forbidden, quadrupole-allowed 1s→3d transition, which can gain intensity through 4p mixing into the 3d orbitals if the molecule deviates from centrosymmetry.[63] In **2**, the pre-edge transition in the Cu K-edge was observed at ∼8980.7 eV, ∼2 eV higher in energy than that observed for Cu(II) complexes, thus falling in the Cu(III) region. In **1**, the pre-edge occurs at 8978.6 eV, demonstrating its Cu(II) nature.[64] To higher energy in the Cu K near-edge region, an intense 1s→4p + ligand-to-metal charge-transfer (LMCT) shake-down transition is observed in **2** (8986.5 eV), which reflects the strong covalent bonding between the metal and ligand orbitals usually associated with Cu(III) complexes.[65,66] In contrast, in **1**, this shake-down transition occurs at 8988.3 eV and is weaker, leading to an almost featureless rising edge reflecting predominant Cu(II) character.

3.2. Cu L-Edge. The normalized Cu L-edge X-ray absorption spectra of **1**, **2**, and the reference complex D_{4h} $(C_4H_8N_3O)_2[CuCl_4]$[29] are presented in Figure 4A. The expanded L_3 regions of the spectra of **1** and **2** are compared to the spectrum of $La_2Li_{1/2}Cu_{1/2}O_4$, an inorganic Cu(III)−oxide **4** (spectrum adapted from ref 29), in Figure 4B. The Cu L-edge spectrum involves the Cu 2p→3d transition and consists of two peaks split by ∼20 eV ($^3/_2$ × the 2p core spin−orbit coupling), with an intensity ratio of ∼2:1 [$J = {}^3/_2$ and $^1/_2$, corresponding to the L_3-edge (∼930 eV) and the L_2-edge (∼950 eV), respectively].[67] The L_2-edge is broadened due to an additional Auger decay channel (Coster−Kronig)[68] of the excited state, which is absent for the

(52) Cowan, R. D. *The Theory of Atomic Structure and Spectra*; University of California Press: Berkeley, 1981.
(53) Butler, P. H. *Point Group Symmetry, Applications, Methods and Tables*; Plenum Press: New York, 1981.
(54) Okada, K.; Kotani, A.; Thole, B. T. *J. Electron Spectrosc. Relat. Phenom.* **1992**, *58*, 325−343.
(55) de Groot, F. M. F.; Fuggle, J. C.; Thole, B. T.; Sawatzky, G. A. *Phys. Rev. B* **1990**, *42*, 5459−5468.
(56) Neese, F.; Olbrich, G. *Chem. Phys. Lett.* **2002**, *362*, 170−178.
(57) Neese, F. ORCA: An Ab Initio, DFT, Semiempirical Electronic Structure Package, 2005.
(58) Schafer, A.; Horn, H.; Ahlrichs, R. *J. Chem. Phys.* **1992**, *97*, 2571−2577.
(59) Schafer, A.; Huber, C.; Ahlrichs, R. *J. Chem. Phys.* **1994**, *100*, 5829−5835.
(60) McGrath, M. P.; Radom, L. *J. Chem. Phys.* **1991**, *94*, 511−516.
(61) Curtiss, L. A.; McGrath, M. P.; Blaudeau, J. P.; Davis, N. E.; Binning, R. C.; Radom, L. *J. Chem. Phys.* **1995**, *103*, 6104−6113.
(62) Krishnan, R.; Binkley, J. S.; Seeger, R.; Pople, J. A. *J. Chem. Phys.* **1980**, *72*, 650−654.
(63) It should be noted that the mechanism of K pre-edge intensities is different from that of L pre-edge intensities (see section 3.2). The K pre-edge transitions are quadrupole allowed and therefore weak. The dominant intensity mechanism in the K pre-edges is metal 4p mixing into the d orbitals. For a more detailed analysis of contributions to K pre-edge intensity, see: Westre, T. E.; Kennepohl, P.; DeWitt, J. G.; Hedman, B.; Hodgson, K. O.; Solomon, E. I. *J. Am. Chem. Soc.* **1997**, *119*, 6297−6314.
(64) Shadle, S. E.; Penner-Hahn, J. E.; H. J., S.; Hedman, B.; Hodgson, K. O.; Solomon, E. I. *J. Am. Chem. Soc.* **1993**, *115*, 767−776.
(65) DuBois, J. L.; Mukherjee, P.; Collier, A. M.; Mayer, J. M.; Solomon, E. I.; Hedman, B.; Stack, T. D. P.; Hodgson, K. O. *J. Am. Chem. Soc.* **1997**, *119*, 8578−8579.
(66) DuBois, J. L.; Mukherjee, P.; Stack, T. D. P.; Hedman, B.; Solomon, E. I.; Hodgson, K. O. *J. Am. Chem. Soc.* **2000**, *122*, 5775−5787.
(67) de Groot, F. M. F. *Physica B* **1995**, *209*, 15−18.
(68) Fuggle, J. C.; Alvarado, S. F. *Phys. Rev. A* **1980**, *22*, 1615−1624.

Table 1. Cu K- and L-Edge X-ray Absorption Edge Energies (eV) and Cu Character in ψ^*_{LUMO}

	Cu K-edge[a]		Cu L-edge[b]		
			2p→3d		
	1s→3d	1s→4p + shake-down	L_3-edge	L_2-edge	Cu character in ψ^*_{LUMO}(% per hole)
$[Cu(O_2)\{HB(3\text{-Ad-}5\text{-}^i Prpz)_3\}]$ (**1**)	8978.6	8988.3[d]	930.8	950.7	20
$[Cu(O_2)(\beta$-diketiminate)] (**2**)	8980.7	8986.5	932.7	952.7	28
$(C_4H_8N_3O)_2[CuCl_4]$ (D_{4h})[e]	8978.6	8986.8	931.0	951.0	61

[a] Energy resolution ~1 eV. [b] Energy resolution ~0.1 eV. [c] **1** and **2** are two-hole systems (see text for detail). [d] The energy is determined from the second-derivative intensity, as the shake-down feature is less pronounced in Cu^{II} systems. [e] Creatininium tetrachlorocuprate(II).

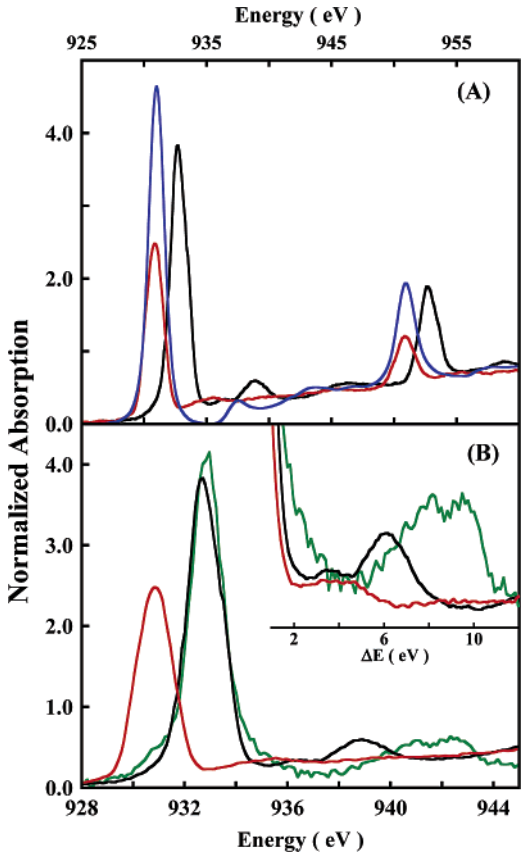

Figure 4. (A) Normalized Cu L-edge XAS spectra of $[^1LCu(O_2)]$ (**1**, red line), $[^2LCu(O_2)]$ (**2**, black line), and D_{4h} $[CuCl_4]^{2-}$ (blue line). The intense peaks at ~930 and ~950 eV represent the L_3-edge ($2p_{3/2}$→3d transition) and the L_2-edge ($2p_{1/2}$→3d transition), respectively. **(**B**)**. Expanded Cu L_3-edge X-ray absorption spectra of $[^1LCu(O_2)]$ (**1**, red line), $[^2LCu(O_2)]$ (**2**, black line), and $La_2Li_{1/2}Cu_{1/2}O_4$ (**4**, green line). Inset: Expanded shake-up region (satellite peak), showing the relative shift in the satellite peak from the main peak (main peak energy positions have been rescaled to 0 eV).

L_3-edge. Both of these pre-edge features are followed by weak 2p→4s and 2p→continuum edge transitions (the intensity of the $\Delta l = +1$ transition is ~30 times higher than that of the $\Delta l = -1$ transition) at ~10 eV higher energy. In the case of Cu(II) $3d^9$ and Cu(III) $3d^8$ complexes, multiplet effects do not redistribute the intensity between the L_3- and L_2-edges (see Supporting Information). Hence, we focus on the L_3-edge energy positions (an analogous trend is observed in the energy shifts in the L_2-edge). The L_3-edges of **1** and D_{4h} $[CuCl_4]^{2-}$ occur at 930.8 and 931 eV,[29] respectively, which are in the range generally observed for normal Cu(II) complexes. The L_3-edge of **2** is at 932.7 eV, which is comparable in energy to that of **4** (~932.9 eV). This ~2 eV shift in the pre-edge is consistent with a change in oxidation state on the Cu and further supports the assignment of **2** as having predominantly Cu(III) character.

Due to the localized nature of the Cu 2p orbital and the fact that a p→d transition is electric-dipole-allowed, the L-edge transition decreases in intensity as the d orbital mixing with the ligand (covalency) increases. This provides a direct probe of Cu 3d ($1 - \beta^2$) character in the $\psi^*_{\beta-LUMO}$.[28,69]

$$\psi^*_{\beta-LUMO} = [1 - \beta^2]^{1/2}|Cu(3d_{x^2-y^2})\rangle - \beta|Ligand(np)\rangle$$

β-LUMO is the spin-down lowest unoccupied molecular orbital. Correlation of the L-edge intensity under the $L_3 + L_2$ peaks with that in D_{4h} $[CuCl_4]^{2-}$ gives a quantitative estimate of the amount of Cu character in an unknown complex.[70] Figure 4A shows a comparison of the total intensity under the L-edge spectra of D_{4h} $[CuCl_4]^{2-}$, **1**, and **2**. Since both **1** and **2** have two unoccupied spin−orbitals (α and β spin of the $3d_{x^2-y^2}$ orbital) with significant Cu character (i.e, two-hole systems), in contrast to the one unoccupied orbital in D_{4h} $[CuCl_4]^{2-}$ (β spin of the $3d_{x^2-y^2}$ orbital), a normalization factor of $^1/_2$ has to be used to quantitatively compare the covalencies of each hole in **1**, **2**, and D_{4h} $[CuCl_4]^{2-}$. Thus, the per-hole L-edge intensities of **1** and **2** (one-half of the intensity in Figure 4A) are much lower than that of D_{4h} $[CuCl_4]^{2-}$, indicating very covalent Cu centers in both complexes. Since the high covalency also leads to shake-up satellite features on the L-edge which redistribute the intensity (vide infra),[71] the total integrated areas were obtained for **1** and **2** and compared to that of D_{4h} $[CuCl_4]^{2-}$.[72] The Cu characters obtained from these total integrated areas are given in Table 1. The reduced Cu character in both of the $[LCuO_2]$ complexes indicates very strong mixing of the O_2^{n-} ligand with the empty Cu d orbital. Further, the total integrated intensity for **2** (which quantitates to 28% per hole metal d character) is more than that of **1** (20%), indicating that **2** has more Cu character, consistent with its Cu(III) description.[22]

4. Analysis

4.1. Multiplet Calculations. Both **1** and **2** are two-hole systems, which can lead to multiplet effects on the L-edge. To gain further insight into the differences in bonding in the two monomeric $[LCuO_2]$ complexes, the TT-Multiplets program was used to fit the mutiplets observed in the L-edge data. The atomic multiplets were simulated by setting the covalent reduction of

(69) In a Cu^{II} system with a $3d^9$ configuration, the highest Cu 3d orbital in a spin-restricted description contains one electron; thus, the description of the ground-state wave function is made as ψ^*_{SOMO}. In the case of both complexes **1** and **2**, the ground state corresponds to a two-hole description and thus is described as $\psi^*_{\beta-LUMO}$.

(70) D_{4h} $[CuCl_4]^{2-}$ has been well characterized by various spectroscopies with 61 ± 4% Cu character in the ψ^*_{SOMO}, which is the same as that for the $\psi^*_{\beta-LUMO}$ in the spin-unrestricted molecular orbital calculations.

(71) Van der Laan, G.; Westra, C.; Haas, C.; Sawatzky, G. A. *Phys. Rev. B* **1981**, *23*, 4369−4380.

(72) Wasinger, E. C.; de Groot, F. M. F.; Hedman, B.; Hodgson, K. O.; Solomon, E. I. *J. Am. Chem. Soc.* **2003**, *125*, 12894−12906.

electron repulsion, β, at 80%. Note that the multiplet splitting is observed in the low-intensity, high-energy satellite peak (~940 eV feature) (Figure 4B, inset), while the main peak is featureless. This indicates that an inverted bonding description is required for the final state (see below). In this case, the ligand field effects alone are limited and contained mostly within the low-intensity satellite peaks. Thus, the data were fit by simultaneously optimizing the LF and charge-transfer (see below) parameters. The molecules are approximately square planar, and so, a D_{4h} effective ligand field was included in the simulations. In each case, the values for the LF parameters Dq, Ds and Dt were systematically varied to find the best-fit simulation. From these LF plus charge-transfer simulations, the most satisfactory 10Dq, Ds, and Dt values were 1.5, 0.1, and 0.15 eV and 2.5, 0.24, and 0.19 eV for complexes **1** and **2**, respectively (Table 2).

The ground-state description in the LF multiplet model is given by a single d^8 configuration which does not include the covalent interactions between the metal d and ligand p orbitals. To allow for bonding, the ground state can be treated within a VBCI model.[73,74] The ground-state wave function of a d^n system can be defined as a linear combination of the d^n configuration and the LMCT, $d^{n+1}\underline{L}$ ($\underline{L}$ = ligand hole) configuration. These are separated by an energy Δ with the two components coupled by the covalent interaction given by T (the transfer integral reflecting orbital overlap). The Hamiltonian and configurations generating this ground state (Ψ_{GS}) and the LMCT excited state (Ψ_{TS}) are given by eqs 1−3:

$$\mathrm{H} = \begin{vmatrix} 0 & T \\ T & \Delta \end{vmatrix} \tag{1}$$

$$\Psi_{GS} = \alpha_0|3d^n\rangle + \beta_0|3d^{n+1}\underline{L}\rangle \tag{2}$$

$$\Psi_{TS} = \beta_0|3d^n\rangle - \alpha_0|3d^{n+1}\underline{L}\rangle \tag{3}$$

These equations are modified in the L-edge final state to include electronic relaxation as given by eqs 4−7:

$$H = \begin{vmatrix} 0 & T_F \\ T_F & \Delta_F \end{vmatrix} \tag{4}$$

$$\Delta_F = \Delta + Q - U \tag{5}$$

$$\Psi_{ES1} = \alpha|\underline{2p}3d^{n+1}\rangle + \beta|\underline{2p}3d^{n+2}\underline{L}\rangle \tag{6}$$

$$\Psi_{ES2} = \beta|\underline{2p}3d^{n+1}\rangle - \alpha|\underline{2p}3d^{n+2}\underline{L}\rangle \tag{7}$$

where Δ_F and T_F are the charge-transfer energy and the electron-transfer matrix element between the two configurations in the final state and Ψ_{ES2} is the charge-transfer final state. The interaction parameter T_F is approximated to be equal to the ground-state parameter T. Q and U are the Cu 2p−3d and 3d−3d Coulomb interactions. Their estimated energy difference is ~ -2 eV;[75,76] thus, Δ_F is approximately $\Delta - 2$ eV. In the case of a Cu(III) system, the value for Δ_F becomes very small and often negative (Scheme 1).[73,76] When Δ_F is negative, the intense L_3 main peak (single peak) at ~930 eV is mainly a transition to the $|2p^53d^{10}\underline{L}\rangle$ configuration, while the weak L_3 satellite peak is mostly due to a transition to the $|2p^53d^9\rangle$ configuration. This is the inverted bonding scheme mentioned above and is consistent with the fact that the main peak is sharp and featureless while the satellite peak exhibits multiplet structure. Using the average energy position and intensity of the L_3 multiplets at ~940 eV as $E_{SATELLITE}$ and $I_{SATELLITE}$, respectively, and those of the 930 eV feature as E_{MAIN} and I_{MAIN}, eqs 8 and 9 give the energy difference and intensity ratio of the main and satellite peaks.

$$E_{MAIN/SATELLITE} = \frac{1}{2}[(\Delta_F^2 + 4T_F^2)^{1/2} \mp \Delta_F] \tag{8}$$

$$\frac{I_{MAIN}}{I_{SATELLITE}} = \frac{(\alpha_0\beta - \beta_0\alpha)^2}{(\alpha_0\alpha + \beta_0\beta)^2} \tag{9}$$

The inset in Figure 4B shows the relative energy shift (from the main peak) and the intensity of the shake-up transitions of the L_3 peak in **1**, **2**, and **4**. The relative energy position and intensity of the shake-up peaks were simulated using the VBCI multiplet program, which determines the values for Δ[77] and T. It should be noted that, although Δ and T are not completely independent of each other, the dominant contribution in

Table 2. Parameters Used in Multiplet Simulations and Ground-State Description of ψ^*_{LUMO}

	crystal field parameters (eV)			ligand field parameters (eV)[a]					$\lvert 3d^n\rangle$ character
	10Dq	Ds	Dt	Δ	T_{B1}[b]	T_{A1}	T_{A1}	T_{B2}	in ψ^*_{LUMO}[c]
1	1.5	0.1	0.15	0.24	0.9	0.35	0.2	0.15	15%
2	2.5	0.24	0.19	0.61	1.7	0.2	0.1	0.1	26%
4	6.0	0.3	0.4[d]	1.9	3.5	1.0	0.2	0.1	32%

[a] The ligand field simulations were performed under D_{4h} symmetry ($T_{B1} = T_{x^2-y^2}$, etc). [b] The dominant contribution in determining the intensity of satellite peak was from T_{B1}. [c] Determined from the projection method. [d] Dt is used to obtain the correct crystal field description.

Scheme 1. Schematic Energy Diagram of the Charge-Transfer Interaction in the Ground and Excited States of a $3d^n$ System Covalently Interacting with a Ligand 2p/3p Orbital[a]

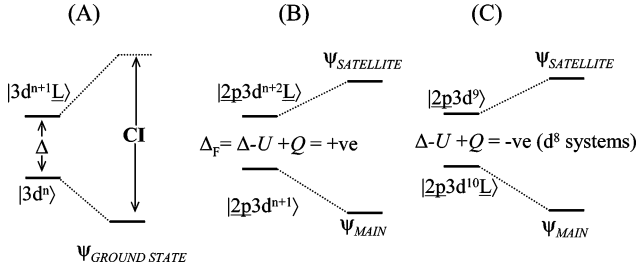

[a] Panel A shows the ground-state configuration interaction. Panels B and C show the excited-state CI mixing with positive and negative charge-transfer energy, respectively.

(73) Hu, Z. W.; Kaindl, G.; Müller, B. G. *J. Alloys Compd.* **1997**, *246*, 177−185.
(74) Van der Laan, G.; Zaanen, J.; Sawatzky, G. A.; Karnatak, R.; Esteva, J. M. *Phys. Rev. B* **1986**, *33*, 4253−4263.
(75) Kaindl, G.; Strebel, O.; A., K.; Schafer, W.; Kiemel, R.; Losch, S.; Kemmlersack, S.; Hoppe, R.; Müller, H. P.; Kissel, D. *Physica B* **1989**, *158*, 446−449.
(76) Mizokawa, T.; Fujimori, A.; Namatame, H.; Akeyama, K.; Kosugi, N. *Phys. Rev. B* **1994**, *49*, 7193−7204.
(77) Δ is defined as the energy difference between the lowest $3d^n$ state and the lowest $3d^{n+1}\underline{L}$ state; however, the input for the multiplet program requires an energy term which represents the energy difference ($E_{AVERAGE}$) of the average energy $3d^n$ and $3d^{n+1}L$ configurations. The perturbation produced due to electron repulsion and multiplet effects is subtracted from $E_{AVERAGE}$ to estimate the accurate Δ value.

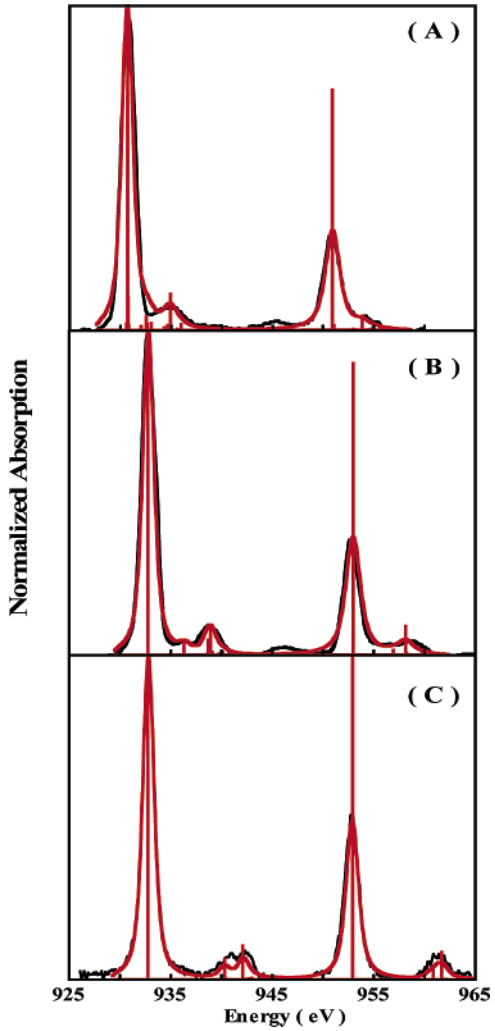

Figure 5. L-edge multiplet simulations. The VBCI simulations of [^{1}LCu(O_2)] (**1**), [^{2}LCu(O_2)] (**2**), and $La_2Li_{1/2}Cu_{1/2}O_4$ (**4**) are shown in panels A, B, and C, respectively. Data are shown in black and simulations in red. The red lines represent the stick spectra and correspond to the transitions with intensity. The stick spectra have been convoluted with a pseudo-Voigt shape to simulate experimental spectra.

determining the energy difference between the main and satellite peaks is Δ and the relative intensity of the peaks is T. In D_{4h} symmetry, there are four interaction terms, T, one for each set of symmetry orbitals: B_{1g}, A_{1g}, B_{2g}, and E_g.[78] The mixing term for B_{1g} ($d_{x^2-y^2}$) is largest due to strong σ overlap of the $d_{x^2-y^2}$ orbital with the ligands. While non-zero values were used for $T(B_{1g})$, $T(E_g)$, $T(B_{2g})$, and $T(A_{1g})$, $T(B_{1g})$ was dominant and is referred to as T in the text below. Figure 5 shows the best-fit multiplet simulations for complexes **1**, **2**, and **4**. Table 2 gives the charge-transfer parameters obtained from the simulations.[79]

The L-edge spectra of **2** and **4** are qualitatively very similar. Although the L-edge spectra of both complexes are shifted up in energy by ~2 eV, indicating a Cu(III) ground state, the small difference in the L_3 (and L_2 (Figure S1, Supporting Information)) edge energy positions (932.7 eV for **2** and ~932.9 eV for **4**) indicates different amounts of ligand hole character in the ground state. The satellite peak is ~8 eV higher in energy than the main peak for **4**, compared to ~6 eV for **2** (Table 3), and the intensity of the satellite peak is higher in **4**. From the VBCI fits, the ground-state wave function in **4** contains more Cu(III) character. The best-fit L-edge simulations (Figure 5 and Table 2) indicate that the $|3d^8\rangle$ character in **4** is 32%, while that in **2** is 26% (Cu character in the ground state is obtained from the projection method developed in ref 71). Thus, **2** is similar to **4** (reflecting their Cu(III) nature) but with increased ligand character in the ground state. In contrast, the L-edge spectra of **2** and **1** are very different in intensity and energy (E_{MAIN} = 932.7 eV in **2** compared to 930.8 eV in **1**). In addition, the satellite peak is ~4 eV higher in energy relative to the main peak for **1**, compared to ~6 eV for **2** (Table 3). The intensity of the satellite peak is lower in **1** compared to that in **2**. The satellite peak for **2** is characterized by a double-peak structure (as for Cu(III) oxides), indicating the presence of multiplet effects which are larger than those for **1** (which shows a weak, broad peak). In the L-edge simulations, the energy position and intensity of the satellite peak restrict the values of Δ and T, and the best-fit simulations for **1** give both a smaller Δ (0.24 eV compared to 0.61 eV for **2**) and a smaller T (0.9 eV compared to 1.7 eV in **2**). Using the projection method, these values give 15% Cu character in the ground state of **1**, compared to 26% for **2**.[72] The covalency values are consistent with the L-edge intensities, showing that there is an increase in electron transfer from O_2^{n-} to Cu for **1** relative to **2**.

Table 3. Energy and Intensity Ratios of Main and Satellite Peaks of the L_3-Edge

	$2p_{3/2} \rightarrow 3d$ (L_3-edge)		
	main peak (eV)	satellite peak (eV)	ΔE^a (eV)
1	930.8	934.7	3.9
2	932.7	938.8	6.1
4	932.9	940.2	8.3

[a] The satellite peak position was determined at the average energy of the multiplet structure.

4.2. Density Functional Theory Calculations. 4.2.1. Geometry Optimization. Broken symmetry spin-unrestricted density functional theory calculations were performed on models derived from the crystal structures of **1** and **2** (see Experimental Section) to correlate with the spectroscopic results to further probe their electronic structure differences. The geometry-optimized structural parameters are in good agreement with the experimental data. The calculated Cu−O and Cu−N bond distances for **1** and **2** are 1.88 and 1.95 Å and 1.86 and 1.90 Å, respectively, compared to the experimental Cu−O and Cu−N bond distances of 1.84 and 1.99 Å and 1.82 and 1.86 Å, respectively. The first coordination bond distances are also consistent with those obtained from extended X-ray absorption fine structure (EXAFS) results.[26] The calculated O−O bond distance for **2** is 1.39 Å, which is in good agreement with the experimental bond distance of 1.39 Å, while the calculated O−O distance for **1** is much longer than the crystallographic distance (1.36 Å compared to 1.22 Å).[19] It has been argued that the crystallographic data underestimate the O−O distance, and spectroscopic data strongly suggest that a longer bond length is appropriate.[22,27] The Cu−O bond distances are comparable for **1** and **2**, while the Cu−N bond distance for **2** is 0.05 Å shorter, indicating a stronger interaction of the diketiminate ligand with the Cu relative to the pyrazole ligand−Cu interaction. The O−O bond distance for **1** is 0.03 Å shorter than that

(78) Eskes, H.; Sawatzky, G. A. *Phys. Rev. B* **1991**, *43*, 119−129.
(79) The published VBCI analysis for the Cu^{III}−oxide, complex **4**, was reproduced in this study. The data were renormalized on the basis of the VBCI results, and the intensity shown in Figure 5 reflects the Cu character obtained from this analysis.

Table 4. Selected Parameters from DFT Calculations

	bond distance (Å)			O–O stretching	β-LUMO composition				natural charge		
	Cu–O	Cu–N	O–O	frequency (cm^{-1})	Cu	O[a]	N[a]	L[b]	Cu	O	N
1	1.88	1.95	1.36	1040	22.7	65.2	9.7	2.4	1.22	−0.58	−1.20
2	1.86	1.90	1.39	990	28.3	54.0	12.7	5.0	1.21	−0.74	−1.30

[a] β-LUMO composition and natural charge represent the sum total on the two O and N atoms. [b] L represents the tripyrazolyl borate and diketiminate ligand systems in **1** and **2**, respectively.

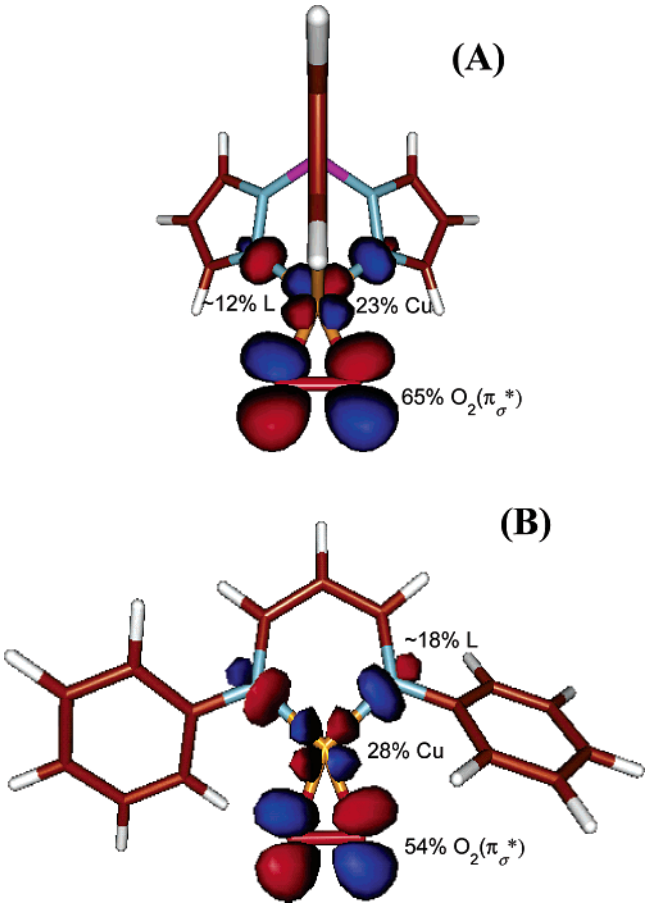

Figure 6. Molecular orbital contour plots of (A) [^{1}LCu(O_2)] (**1**) and (B) [^{2}LCu(O_2)] (**2**). The contour plots have been generated in MOLDEN. The Mulliken population of ψ^*_{LUMO} is shown next to the relevant atom(s). L denotes trispyrazolyl borate and β-diketiminate in **1** and **2**, respectively.

for **2**, consistent with its more superoxide-like character compared to the more peroxide-like character for **2**.

4.2.2. Frequencies. To further correlate to the experimental assignments of **1** and **2**, frequency calculations were performed and are presented in Table 4. The O−O stretching frequencies obtained from the BP86 DFT calculations did not have appreciable mixing with other vibrational modes and hence reflect the O−O bond. The O−O stretching frequencies obtained for **1** and **2** are 1040 and 990 cm^{-1}, respectively, which are in reasonable agreement with the experimentally obtained frequencies of 1043 and 968 cm^{-1} for complexes **1** and **2**, respectively.

4.2.3. Ground-State Wave Functions. The MO surface contour plots of the calculated singlet ground states of both **1** and **2** are presented in Figure 6. DFT calculations using BP86 give ground-state descriptions that are in reasonable agreement with experimental ground-state properties, in particular the singlet nature of **1**. Table 4 summarizes the compositions of selected spin-down molecular orbitals for both molecules. The Cu $d_{x^2-y^2}$ characters calculated for the ψ^*_{LUMO} are 22.7% and 28.3% for **1** and **2**, respectively, consistent with the experimental values obtained from L-edges (20% and 28% in **1** and **2**, respectively. This indicates that both systems have highly covalent Cu centers. The contour plots in Figure 6 show extensive delocalization over the Cu−O_2^{n-} moiety in both complexes. The O_2^{n-} characters in the β-LUMOs of **1** and **2** are 65.2% and 54.0%, respectively. The equatorial nitrogen atoms contribute 9.7% and 12.7% (per hole) in **1** and **2**, respectively (the total contributions of trispyrazolyl borate and β-diketiminate ligands are 17.7% and 12.3%, respectively), reflecting the greater donor strength of the bidentate β-diketiminate ligand in **2**.

4.2.4. Electronic Structure Descriptions. In these approximately planar geometries, the most destabilized d orbital is $d_{x^2-y^2}$ (see Figure 2 for molecular coordinate system). The highest-lying filled molecular orbitals in the free O_2^{n-} moiety is the π^* set, which split into π^*_σ and π^*_ν upon bonding with Cu. The π^*_ν orbital is perpendicular to the molecular plane; hence, it does not have significant overlap with the Cu $d_{x^2-y^2}$ orbital. The in-plane π^*_σ orbital forms strong σ bonds with the Cu $d_{x^2-y^2}$ orbital, destabilizing it to higher energy. The NPA charge on the O_2 moiety in **2** is more negative than in **1** (Table 4, −0.74 for **2** and −0.58 for **1**), consistent with their assignments as peroxide and superoxide, respectively, which is supported by the O−O stretching frequencies and Cu K-edge data. This is also consistent with the larger Cu character in the ψ^*_{LUMO} for **2** compared to **1**.

4.2.5. K-Edge Energy Shifts. Cu K-edge and L-edge X-ray absorption spectra exhibit characteristic shifts of the pre-edge to higher energy on going from **1** to **2**, which indicate an increase in oxidation state. The K- and L-edge shift magnitudes are very similar (K-edge, ~2.2 eV; L-edge, ~1.9 eV). To correlate these pre-edge energy shifts with electronic structure changes on going from a Cu(II) to a Cu(III) complex, 1s→3d and 2p→3d TD-DFT calculations were performed on **1** and **2**. Note that these calculations do not include relativistic effects, so only relative energies are considered. The experimental trend in the K pre-edge energy shift (ΔE_{2-1} = 2.2 eV) is reproduced, although the TD-DFT calculated shift is 0.6 eV. The trend in the L-edge shift (ΔE_{2-1} = 1.9 eV) is also reproduced, but again the calculated energy shift is lower, at 0.5 eV. Interestingly, the calculated ΔE_{2-1} values for both L- and K-edges are very similar (similar to the experimental shifts).

There are two potential contributions to the shifts observed in the Cu K and L pre-edge energies: Q^{Cu}_{mol}, the charge on the Cu atom in the molecule, and the ligand field strength, LF.[80] An increase in Q^{Cu}_{mol} might be expected to shift the pre-edge to higher energy due to a larger contraction of the core levels relative to the valence levels. An increase in LF would destabilize the ψ^*_{LUMO} and increase the pre-edge energy.

(80) Randall, D. W.; DeBeer George, S.; Holland, P. L.; Hedman, B.; Hodgson, K. O.; Tolman, W. B.; Solomon, E. I. *J. Am. Chem. Soc.* **2000**, *122*, 11632−11648.

Table 5. Selected DFT Parameters and Comparison of Cu K-Edge and TD-DFT Transition Energies

	DFT (Gaussian)			1s→3d transition (eV)		
	bond distance (Å)	Mulliken charge			TD-DFT (ORCA)[a]	
	Cu–$N_1(N_2)$	Cu	$N_1(N_2)$	Cu K-edge	TZVP	6-311G*
$[Cu^{II}L]^{2-}$	1.94(1.95)	1.04	−0.71(−0.82)	8978.7	8749.2	8748.2
$[Cu^{III}L^*]^-$	1.94(1.95)[b]	1.15	−0.71(−0.82)		8749.4	8748.4
$[Cu^{III}L]^-$	1.85(1.86)	1.18	−0.74(−0.83)	8980.8	8750.1	8749.2

[a] DFT underestimates the core binding energy; the energies are reported for relative comparison. [b] The bond distances in $[Cu^{III}L^*]^-$ (single-point calculation) are identical to those in $[Cu^{II}L]^{2-}$.

Scheme 2. Schematic Representation of the Changes in the 1s, 2p, and 3d Orbital Energies upon One-Electron Oxidation of $[Cu^{II}L]2-$ to $[Cu^{III}L^*]-$ and to $[Cu^{III}L]^{-a}$

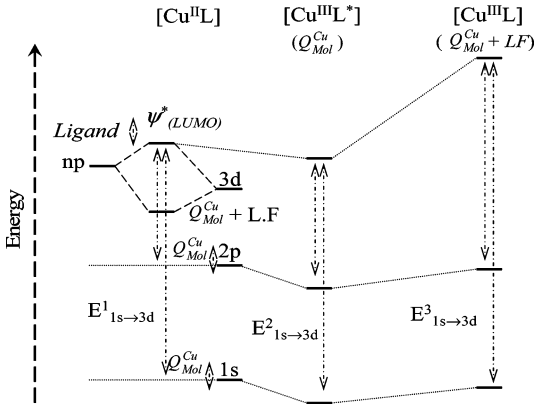

[a] The formation of $[Cu^{III}L^*]^-$ involves a change in Z_{eff}, while formation of $[Cu^{III}L]$ involves a change in both LF and Z_{eff}, indicating that LF effects have a dominant contribution to the edge shift and $E^1 \approx E^2 < E^3$. LF = ligand field, np = 2p(O).

However, the LF and Q^{Cu}_{mol} contributions are coupled, as an increase in LF reflects stronger bonding between the metal and ligand orbitals, which will tend to decrease Q^{Cu}_{mol}.

To evaluate the relative contributions of LF and Q^{Cu}_{mol} to the pre-edge transition energies, 1s→3d TD-DFT calculations were performed on two additional mononuclear complexes, $(PPh_4)_2$-$[Cu^{II}L]$ and $(PPh_4)[Cu^{III}L]$ (where L = bis(methylamide) derivative of *N*,*N*′-*o*-phenylenebis(oxamate)),[81] which differ by one electron oxidation. This pair of molecules is useful as a reference as they are both approximately square-planar, N-ligating systems, similar to **1** and **2**, and their experimental Cu K-edge data are available.[66] The experimental shifts in the Cu K pre-edge energy in these complexes follow the expected trend ($Cu^{III}_{pre-edge} - Cu^{II}_{pre-edge} \approx 2$ eV). The K-edge spectra of these complexes have been published and are reproduced in Figure S2 (Supporting Information) for reference.[66] Structural parameters and Mulliken atomic charges obtained from DFT calculations on $[Cu^{II}L]^{2-}$, $[Cu^{III}L]^-$, and $[Cu^{III}L^*]^-$ are given in Table 5. $[Cu^{III}L^*]^-$ corresponds to an un-relaxed ionized state of the molecule in which the geometric relaxation due to one-electron oxidation has been restricted (Scheme 2) by using the same Cu−N bond distances as in $[Cu^{II}L]^{2-}$. The Cu−N bond distances are 1.94 and 1.95 Å in the optimized structure of $[Cu^{II}L]^{2-}$ and 1.85 and 1.86 Å in the optimized structure of $[Cu^{III}L]^-$. These distances are in excellent agreement with the X-ray crystal structure data (1.93 and 1.96 Å for $[Cu^{II}L]^{2-}$ and 1.84 and 1.88 Å for $[Cu^{III}L]^-$). In addition, the molecules are essentially square planar with no D_{2d} distortion. Thus, a one-electron oxidation of $[Cu^{II}L]^{2-}$ to $[Cu^{III}L]^-$ results in a ∼0.1 Å decrease in the ligand−Cu bond distances. The charge on Cu increases on going from $[Cu^{II}L]^{2-}$ to $[Cu^{III}L^*]^-$ (1.04 to 1.15), but on going from $[Cu^{III}L^*]^-$ to $[Cu^{III}L]^-$ the change is very small (1.15 to 1.18). The charge on the Cu is reflected in the Cu character in the β-LUMO orbital, which contains 52%, 68%, and 69% Cu character in $[Cu^{II}L]^{2-}$, $[Cu^{III}L^*]^-$, and $[Cu^{III}L]^-$, respectively. The average charges on the N atoms, which are very similar for the three complexes, are −0.76, −0.76, and −0.78 for $[Cu^{II}L]^{2-}$, $[Cu^{III}L^*]^-$, and $[Cu^{III}L]^-$, respectively.

TD-DFT calculations of the 1s→3d transition were performed on the optimized structures obtained from the DFT calculations using ORCA.[56,57] This ensures that the ligand fields between $[Cu^{II}L]^{2-}$ and $[Cu^{III}L^*]^-$ are similar. Additionally, on going from $[Cu^{III}L^*]^-$ to $[Cu^{III}L]^-$, where the molecule has now been geometry optimized to allow for structural relaxation, the charge on Cu remains the same (Table 5). Thus, the 1s→3d transition energies obtained from the TD-DFT calculations should predominantly reflect the effect of a change in charge on Cu on going from $[Cu^{II}L]^{2-}$ to $[Cu^{III}L^*]^-$ and a change in ligand field on going from $[Cu^{III}L^*]^-$ to $[Cu^{III}L]^-$. The transition energies obtained from the 1s→3d TD-DFT calculations are given in Table 5. The trend observed for the experimental transition energies is reproduced by the TD-DFT calculations, and the shift due to one-electron oxidation is ∼1 eV (compared to ∼2 eV for the experimental data). However, the change in 1s→3d transition energy on going from $[Cu^{II}L]^{2-}$ to $[Cu^{III}L^*]^-$ is only ∼0.2 eV, while the change on going from $[Cu^{III}L^*]^-$ to $[Cu^{III}L]^-$ is ∼0.8 eV. Thus, although most of the Q^{Cu}_{mol} increase occurs on going from $[Cu^{II}L]^{2-}$ to $[Cu^{III}L^*]^-$ (11%), there is only a very small shift in calculated K pre-edge energy. However, while there is almost no change in Q^{Cu}_{mol} (∼1%) on going from $[Cu^{III}L^*]^-$ to $[Cu^{III}L]^-$, there is a significant change in the pre-edge energy. This indicates that the contribution of Q^{Cu}_{mol} to the pre-edge transition energy is, in fact, very small and that these energy shifts are dominated by changes in LF. This is consistent with the observation that similar shifts are observed in L and K pre-edge transition energies between **1** and **2**. Thus, the change in Q^{Cu}_{mol} leads to similar energy shifts in the Cu 1s, 2p, and 3d orbitals and the pre-edge shift observed is predominantly due to LF. In **1** the N-containing ligand system is trispyrazolyl borate, which forms two fairly weak Cu−N bonds in the equatorial position at ∼2 Å (a weak ∼2.25 Å Cu−N bond is also present).[82] In contrast, the partial negative charge on the nitrogens of the β-diketiminate ligand leads to the formation of strong Cu−N bonds (at ∼1.86 Å) in **2**, increasing the ligand field and destabilizing the $d_{x^2-y^2}$ orbital relative to that in **1**.

(81) Ruiz, R.; Surville-Barland, C.; Aukauloo, A.; Anxolabéhère-Mallart, E.; Journaux, Y.; Cano, J.; Munõz, M. C. *J. Chem. Soc., Dalton Trans.* **1997**, 745−751.

(82) The aromatic pyrazole groups do not significantly participate in the bonding of trispyrazolyl borate with Cu.

This is consistent with DFT calculations which indicate larger nitrogen character (18% per hole) in **2** relative to **1** (12% per hole) This is also consistent with the [LCu-thiolate] study by Randall et al.,[80] which showed, using a combination of magnetic circular dichroism (MCD) and XAS studies, that the β-diketiminate ligand interacts more strongly with Cu, resulting in larger destabilization of the $d_{x^2-y^2}$ orbital relative to the trispyrazolyl borate ligand. This increase in ligand field leads to the large shift observed in the K pre-edge of **2** relative to **1**.

5. Discussion

5.1. Nature of Cu−O_2 Bonds. Resonance Raman spectroscopic studies and theoretical calculations have been performed on complexes **1** and **2** which indicate their respective superoxide vs peroxide nature.[22,25−27,83,84] In this study, Cu K- and L-edge data on **1** and **2**, combined with the results obtained from VBCI analysis of the L-edge spectra, are used to experimentally probe differences in the Cu−O_2^{n-} bonding and to evaluate the nature of the Cu−O_2^{n-} bond in **1** and **2**. Quantitating the total integrated intensities under the L-edge peaks (Figure 4A) indicates that both complexes are very covalent and that **1** has a ground state with 20% Cu character, while for **2** the Cu character is 28%. Further, the L-edge of **2** has a larger gap between the main and satellite peaks and higher intensity of the satellite features at ~935−940 eV, which also exhibit more multiplet structure. VBCI simulations of these L-edge spectra reproduce the strongly covalent nature of the ground states, with more d^8 Cu(III) character in **2**. In the VBCI framework, two factors contribute to the covalent mixing of the d^8 Cu(III) ground state with the charge-transfer excited state: (i) a small Δ term where the two interacting states are close in energy and (ii) a large T term for the interaction (L−M overlap) between them. The Δ and T values for **1** and **2** obtained from the best-fit VBCI simulations are 0.24 and 0.9 eV and 0.61 and 1.7 eV, respectively. The higher value of T for **2** more than compensates for its larger Δ, leading to a net increase in the amount of Cu character in the ground-state wave function relative to **1**.

DFT calculations are consistent with previous theoretical studies[27] and support the experimental results and analysis. The experimental trends in the O−O stretching frequencies of 1043 and 948 cm^{-1} for **1** and **2** are reproduced by the calculations (1040 cm^{-1} for **1** and 990 cm^{-1} for **2**) and support the electronic structure description of **1** and **2** as superoxide and peroxide copper complexes, respectively. The experimental trend in the Cu character in the ψ^*_{LUMO} is also reproduced reasonably well. The differences in the ligand character in the ψ^*_{LUMO} indicate that the planar ring system of the β-diketiminate and anionic charge localization on the N's lead to a very strong bonding interaction with Cu and significant charge donation from the β-diketiminate, stabilizing the Cu(III) state. The strong interaction of β-diketiminate with Cu relative to tris(pyrazolyl)-hydroborate was described in a spectroscopic study by Randall et al.,[80] in which it was demonstrated that the increased donation of the β-diketiminate ligand weakens the Cu−thiolate bond relative to the tris(pyrazolyl)hydroborate ligand system. This result was invoked in a theoretical study on derivatives of **1** and **2** by Cramer et al.,[27] which indicated that an electron-rich metal tends to form a peroxide species.

In the Cu−thiolate study by Randall et al.,[80] although the thiolate character in the ψ^*_{SOMO} changes significantly, the Cu character remains very similar in both complexes. In contrast, in the Cu−O_2^{n-} systems, the interaction between the π^*_σ orbital on O_2^{n-} and the $3d_{x^2-y^2}$ orbital on Cu leads to a very covalent two-hole system, which results in Cu(II)−superoxide or Cu(III)−peroxide character, depending on the relative contributions of Cu and O to the ψ^*_{LUMO}. It is important to note that, in contrast to the Cu^{II}−thiolate systems, the Cu characters in **1** and **2** are different. This difference arises from the presence of additional electron repulsion on going from a d^9 to a d^8 system, which localizes Cu character in the ψ^*_{LUMO}.

This difference in the composition of the ψ^*_{LUMO} indicates that the ligand environment regulates the O_2^{n-} character in the ground state. The amount of O_2^{n-} character in the ψ^*_{LUMO} is larger in **1** (65% π^*_σ) than that in **2** (54% π^*_σ). This is critical in terms of reactivity in PHM and DβM, as it indicates that the frontier molecular orbital of a superoxide-like species would be activated toward H-atom abstraction.[11] The ligand system of the Cu_M site in PHM (2 N(His), 1 S(Met), and 1(H_2O)) is similar in ligand field to the trispyrazolyl ligation in **1**.[10,17] This is consistent with various experimental and theoretical studies on PHM, which implicate (and possibly observe) the formation of a [Cu^{II}−O_2^-] intermediate which is tuned toward substrate hydroxylation.[3,11,18] Thus, this study provides insight into the ligand environment contribution to the formation of a [Cu^{II}−O_2^-] intermediate in PHM (and DβM) and in tuning its reactivity.

5.2. Contributions to Pre-edge Energy Shifts. L-edge intensity is a direct probe of the total metal character in the β-LUMO and thus directly reflects the charge on the metal atom in the molecule (Q^M_{mol}).[85] It has been shown by X-ray photoelectron spectroscopy that changes in Q^M_{mol} result in large shifts in the ionization energies, referred to as chemical shifts, which reflect the formal oxidation state of the atom in the molecule. This might indicate that the L pre-edge energy should increase with increase in the relative L-edge intensity. Figure 7A shows a comparison of the Cu L_3 pre-edges of [Cu(TMPA)(OH_2)]-(ClO_4)$_2$ (**3**), **2**, and the blue copper site in plastocyanin. The normalized L-edge intensities of **3**, **2**, and plastocyanin are 55%, 56% (28% per hole), and 42%, respectively. The effective charge on copper is quite different between **3** and plastocyanin, yet the pre-edge energy positions for both occur at 930.8 eV. In contrast, the charge on copper is the same for **2** and **3**, while the pre-edge for **2** is at 932.7 eV, ~2 eV higher than for **3**. Thus, the L-edge energy positions do not directly reflect Q^{Cu}_{mol}. The calculations on [$Cu^{II}L]^{2-}$, [$Cu^{III}L^*]^-$, and [$Cu^{III}L]^-$ presented in section 4.2.5 also indicate that there is very little effect on the edge energy due to the change in charge on the copper and the dominant contribution to the edge shift is from the increased ligand field at the Cu(III) in the complex.

The effect of change in charge on an atom in a molecule (ΔQ^M_{mol}) on the 2p and 3d orbitals has been modeled.[86,87] This ΔQ^M_{mol} modeling was extended in this study to obtain the relative change in 1s and 2p core and 3d valence orbital energies in a copper atom due to ΔQ^{Cu}_{mol}. The correlation of the core(1s):

(83) Pantazis, D. A.; McGrady, J. E. *Inorg. Chem.* **2003**, *42*, 7734−7736.
(84) Gherman, B. F.; Cramer, C. J. *Inorg. Chem.* **2004**, *43*, 7281−7283.
(85) This is valid when metal 4s and 4p do not contribute significantly to bonding.
(86) Kennepohl, P.; Solomon, E. I. *Inorg. Chem.* **2003**, *42*, 679−688.
(87) Kennepohl, P.; Solomon, E. I. *Inorg. Chem.* **2003**, *42*, 689−695.

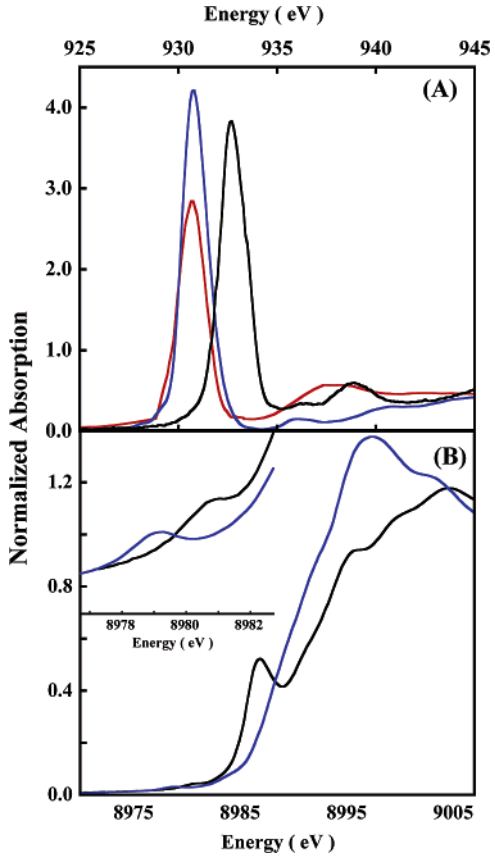

Figure 7. (A) Normalized Cu L_3-edge spectra of $[Cu^{II}(TMPA)(OH_2)](ClO_4)_2$ (**3**, blue line), plastocyanin (red line), and $[^2LCu(O_2)]$ (**2**, black line). (B) Normalized Cu K-edge spectra of $[Cu^{II}(TMPA)(OH_2)](ClO_4)_2$ (**3**, blue line) and $[^2LCu(O_2)]$ (**2**, black line). Inset: Expanded pre-edge region (1s→3d transition).

core(2p) orbital energies was found to be ~1:1, while the core: valence correlation is ~0.9:1 (Figure S3, Supporting Information). These results are consistent with XPS data which show that, over a series of compounds with different Q^M_{mol} values (due to differences in formal oxidation state), the chemical shifts observed in the valence and core levels are approximately the same. Since metal K and L pre-edges probe transitions between two bound states, the energy shift due to a change in Q^M_{mol} is small.[88,89] Thus, the energy shifts associated with pre-edges reflect contributions from the ligand field. Figure 7B shows a comparison of the Cu K-edges of **2** and **3**. The K pre-edge energy shift is ~2 eV, which is similar to the L pre-edge energy shift (Figure 7A). Since the ligand field dominantly affects the valence orbitals involved in bonding, the shifts in the Cu K- and L-edges are necessarily very similar (within resolution).

5.3. Electronic Structure of Cu^{III} Compounds. Cu(III) complexes are important chemical oxidants, implicated as intermediates in oxidative processes, and comprise an important class of superconductors.[66,73,78,90] In recent years, a number of Cu(III) complexes have been characterized,[91−93] and crystal structures and EXAFS data on these indicate that the first-shell Cu(III)−L distance is 0.1 Å shorter than in similar Cu(II) complexes. In an extensive X-ray absorption Cu K-edge study, DuBois et al.[66] have shown that the Cu K-edges of Cu(III) complexes look dramatically different from those of Cu(II) complexes and have assigned the ~2 eV pre-edge shift (~8979 eV to ~8981 eV) as a signature of a unit increase in oxidation state. It is shown in the present study that this shift in the pre-edge energy position for both K- and L-edges is, in fact, dominated by ligand field contributions. The L-edge intensity of **2**, a Cu(III) complex, is very similar to that of normal Cu(II) complexes (Figure 7A), indicating that their Q^{Cu}_{mol} values are very similar. This similarity in L-edge intensity, combined with the 0.1 Å shortening of Cu−L bonds, indicates that Cu(III) complexes have very strong covalent bonds. Hence, the charge built up by the one-electron oxidation of a Cu(II) to a Cu(III) species is neutralized by extensive charge donation by the ligand framework to the metal. This reflects Pauling's electroneutrality principle.

In summary, the electronic structures of two mononuclear $LCuO_2$ systems, **1** and **2**, have been evaluated using Cu K- and L-edge XAS coupled with calculations. The XAS data, particularly the L-edge intensities, clearly demonstrate the Cu(II)−O_2^- and Cu(III)−O_2^{2-} natures of **1** and **2**, respectively. These differences reflect the difference in donor interactions of L with Cu (greater in **2**) coupled with the increased electron repulsion in these two-hole systems. Ligand field and Q^{Cu}_{mol} contributions to Cu K- and L- pre-edge shifts have been evaluated using DFT and TD-DFT calculations and through correlation to XPS data. It is found that, for bound-state transitions, the pre-edge energy shift is dominated by the ligand field and is less affected by a change in Q^{Cu}_{mol}. Finally, it is shown that Cu(III) compounds can have Q^{Cu}_{mol} values similar to those of Cu(II) complexes due to increased donor interaction with the ligand to compensate for the increased charge on the metal center.

Acknowledgment. This research was supported by NIH Grants DK-31450 (E.I.S.), RR-01209 (K.O.H.), and GM-47365 (W.B.T.) and the JSPS Grants 14350471 and 17350043 (K.F.). SSRL operations are funded by the U.S. Department of Energy, Office of Basic Energy Sciences. The Structural Molecular Biology program at SSRL is supported by the National Institutes of Health, National Center for Research Resources, Biomedical Technology Program, and by the Department of Energy, Office of Biological and Environmental Research. The authors thank Frank de Groot for assistance with the multiplet program, Frank Neese for the supply of and assistance with the ORCA program, Kenneth D. Karlin for the supply of **3**, and Z. Hu for providing the L-edge spectra of **4**.

Supporting Information Available: Cu L-edge XAS spectra of **1**, **2**, and **4**; Cu K-edge spectra of $[CuL](PPh_3)_2$ and $[CuL](PPh_3)_2$; DFT-calculated Cu 1s, 2p, and 3d orbital relationship with change in Q^{Cu}_{mol}; VBCI simulation parameters for **1** and **2**; full author list for refs 26 and 38. This material is available free of charge via the Internet at http://pubs.acs.org.

JA0615223

(88) Fadley, C. S.; Hagström, S. B.; Klein, M. P.; Shirley, D. A. *J. Chem. Phys.* **1968**, *48*, 3779−3794.
(89) Christ, B. V. *Handbook of Monochromatic XPS Spectra*; John Wiley & Sons: New York, 2000.
(90) Hu, Z.; Kaindl, G.; Warda, S. A.; Reinen, D.; de Groot, F. M. F.; Müller, B. G. *Chem. Phys.* **1998**, *232*, 63−74.
(91) Diaddario, L. L.; Robinson, W. R.; Margerum, D. W. *Inorg. Chem.* **1983**, *22*, 1021−1025.
(92) Mahapatra, S.; Halfen, J. A.; Wilkinson, E. C.; Pan, G. F.; Wang, X. D.; Young, V. G.; Cramer, C. J.; Que, L., Jr.; Tolman, W. B. *J. Am. Chem. Soc.* **1996**, *118*, 11555−11574.
(93) Mahadevan, V.; Hou, Z. G.; Cole, A. P.; Root, D. E.; Lal, T. K.; Solomon, E. I.; Stack, T. D. P. *J. Am. Chem. Soc.* **1997**, *119*, 11996−11997.